Tunable viscous layers in Corbino geometry using density junctions

Ramal Afrose [1], Aydın Cem Keser [2,3], Oleg P. Sushkov [3,4] and Shaffique Adam [1,5,6,7,8]

[1] *Department of Physics, Faculty of Science, National University of Singapore, Science Drive 3, Singapore 117542, Singapore*

[2] *CSIRO, Bradfield Road, West Lindfield NSW 2070, Australia*

[3] *Australian Research Council Centre of Excellence in Low-Energy Electronics Technologies, The University of New South Wales, Sydney 2052, Australia*

[4] *School of Physics, University of New South Wales, Kensington, NSW 2052, Australia*

[5] *Centre for Advanced 2D Materials, National University of Singapore, 6 Science Drive 2, Singapore 117546, Singapore*

[6] *Department of Materials Science and Engineering, National University of Singapore, 9 Engineering Drive 1, Singapore 117575, Singapore*

[7] *Yale-NUS College, 16 College Avenue West, Singapore 138527, Singapore*

[8] *Department of Physics, Washington University in St. Louis, St. Louis, Missouri 63130, USA*

(Received 2 May 2024; revised 1 August 2024; accepted 19 August 2024; published 6 September 2024)

In sufficiently clean materials where electron-electron interactions are strong compared to momentum-relaxing scattering processes, electron transport resembles the flow of a viscous fluid. We study hydrodynamic electron transport across density interfaces (n-n junctions) in a 2DEG in the Corbino geometry. From numerical simulations in COMSOL using realistic parameters, we show that we can produce tunable viscous layers at the density interface by varying the density ratio of charge carriers. We quantitatively explain this observation with simple analytic expressions together with boundary conditions at the interface. We also show signatures of these viscous layers in the magnetoresistance. Breaking down viscous and Ohmic contributions, we find that when the outer radial region of the Corbino has higher charge density compared to the inner region, the viscous layers at the interface serve to suppress the magnetoresistance produced by momentum-relaxing scattering. Conversely, the magnetoresistance is enhanced when the inner region has higher density than the outer. Our results add to the repertoire of techniques for engineering viscous electron flows, which hold a promise for applications in future electronic devices.

DOI: 10.1103/PhysRevB.110.125409

I. INTRODUCTION

In lieu of the Drude flow in conventional conductors, electrons flow like a viscous fluid when collisions among them become the dominant scattering mechanism [1–4]. This hydrodynamic regime has long remained elusive in experiments due to want of fabrication of sufficiently clean materials where electron-electron interactions are strong compared to momentum-relaxing scattering. However, the advent of ultrahigh mobility 2D electron systems has bridged this gap. Several effects of viscous electron flow like negative nonlocal resistance [5,6], electron-hole drag [7], vorticity [8,9], Poiseulle flow [10,11], superballistic conductance through point contacts [12–14], and violation of Widemann-Franz law [15–19] are predicted and have also been observed. With a magnetic field, more unconventional effects like negative magnetoresistance [20–25], Hall viscosity [26,27] and giant anomalous photoresistivity [28–32] have been seen.

Two main geometries that have been used to study electron transport at the mesoscopic scale are the Hall bar and the Corbino ring. Unlike the Hall bar, the Corbino does not have edges except for the source and drain terminals. This distinctive feature makes it an attractive setup to study bulk states in the quantum Hall regime, since quantum Hall transport measurements in the more conventional Hall bar geometry are dominated by contribution from edge currents. In addition, due to transverse Hall currents in a magnetic field, the Corbino makes magnetoresistance a feasible probe to study hydrodynamics [33–36]. For example, Ref. [33] derives a quadratic-in-field magnetoresistance in a 2DEG Corbino ring (e.g., in GaAs heterojunctions), and shows that an applied electric field is expelled from the bulk of the sample in spite of viscous dissipation. However, at low carrier densities, due to nonvanishing temperature gradients this is no longer true [37,38]. Reference [34] shows how viscosity affects magnetoresistance in charge neutral graphene Corbino ring assuming no-slip and no-stress leads. Reference [35] extends the study to low-density and the high-density limiting cases and show that although the simple expression of Ref. [33] is valid in the high-doping Fermi liquid regime, additional contributions appear near neutrality point. Thermoelectric coefficients calculated in the ballistic limit [39] show signatures of transition from quantum Hall transport to incoherent transport. Since we are only concerned with the high charge density transport regime, we use the formalism of Ref. [33].

The situation is very different in the Hall bar geometry, where magnetoresistance is either very weak (for small fields) or is complicated by several factors such as change in viscosity [20,26], size of cyclotron orbit compared to channel width [40,41], edge currents [42], etc. Moreover, the presence of edges introduces an unknown boundary condition which effects the flow [43]. Recent efforts have been made to mitigate this problem by making samples with perfect-slip boundaries. This was done by inducing an electron channel in a GaAs heterostructure by applying a bias from a top gate instead

TABLE I. Value of parameters of 2DEG used for simulation of hydrodynamic flow. Parabolic dispersion $\epsilon = p^2/(2m^*)$, with spin degeneracy $g_s = 2$ is assumed.

Parameter	Description	Value	Parameter	Description	Value
n_1	charge carrier density	2×10^{11} cm^{-2}	m^*	effective electron mass	$0.067m_e = 6.1 \times 10^{-32}$ kg
B	Applied magnetic field	20 mT	l_{ee}	e-e scattering length for $n = n_1$	300 nm
μ	mobility	2×10^6 cm^2/(V s)	l_{mr}	momentum-relaxing scattering length	14.8 μm
D_1	Gurzhi length for $n = n_1$	1.05 μm	$2d$	width of interface	$0.2D_1 = 210$ nm
r_1	radius of inner contact	$4D_1 = 4.2$ μm	r_2	radius of outer contact	$15D_1 = 15.8$ μm

of chemical doping. There, viscous effects were artificially re-introduced by modifying the geometry of the channel [22], or by means of magnetic modulation [44–46]. The Corbino geometry provides an alternative solution to the problem of boundary conditions by completely eliminating boundaries except for contacts at source and drain.

Experiments on the Corbino in graphene have directly probed the existence of viscous layers localised at the input and output terminals [47]. These layers are approximately as wide as the "Gurzhi length" D, that is, the momentum diffusion length arising from combination of momentum relaxing and momentum conserving e-e scattering, and defined as $D = \sqrt{l_{mr} l_{ee}}/2$. Due to the high mobility of 2DESs with respect to the metallic leads, and due to rough surfaces of the leads over microscopic length scales, electron flow into and out of the sample is almost always normal. In this paper, we explore the possibility of a situation where the injected velocity has a tunable tangential component, by considering electron flow through two regions of different density (n-n junction) in the Corbino geometry. Away from the boundaries, viscous forces cease to operate and the electron transport assumes Drude character. The Drude flow depends on the charge density of carriers and is different on either side of the junction. At a no-stress interface of two densities, the tangential flow must be continuous, forcing the velocity to reduce to a common value and leading to formation of viscous layers. The strength of these layers is directly proportional to the mismatch between the interface velocity and the Drude velocity in the bulk. Therefore, by tuning the gate bias, we can easily realize viscous layers of varying lengths.

Manipulating viscous electron flow at mesoscopic length scales is an actively pursued endeavour. Recent works studying hydrodynamic flows through different channel geometries [48] find that effective channel width can change for different geometries while the microscopic scattering parameters are unaffected. Although boundary conditions are never perfectly determined microscopically, a perfect no-slip boundary can be realised over larger length scales by considering current flowing through a series of constrictions [49]. Reference [43] show that slip length at the boundaries can vary with temperature in a nontrivial way, while other studies [50] demonstrate how nonlinear hydrodynamic effects like Bernoulli effect, Eckart streaming and Rayleigh streaming can be realised in special scenarios. Our proposal of a gate-tunable viscous layer could be used for easy electrical manipulation of thermal dissipation at interfaces and adds to the growing repertoire of methods for viscous flow engineering.

The plan of the paper is as follows. In Sec. II, we show the emergence of distinct viscous layers at a density interface from numerical simulation of compressible Stokes flow in COMSOL. We next present an analytical explanation of this result in Sec. III using simple expressions derived from the more complicated exact solution. We show that we can piecewise model the flow and match them at the interface by using simple interface conditions, which we derive in Sec. IV. Then, in Sec. V, we show signatures of these viscous layers in the magnetoresistance. We also decompose the Ohmic and viscous contributions with analytic expressions. Finally, we end with a summary of our findings in Sec. VI.

II. TUNABLE VISCOUS LAYERS AT DENSITY INTERFACE

In this section, we present results from numerical simulation of hydrodynamic flow across a density gradient and show that viscous layers can be induced at the interface of different density regions. In the parameter window favoring hydrodynamic regime of transport, the local conservation laws of particle number and momentum which govern the electron flow take the form of the equation of continuity and the Stokes equation [22]

$$\nabla \cdot (n\mathbf{u}) = 0, \tag{1a}$$

$$ne(\mathbf{E} + \mathbf{u} \times \mathbf{B}) + \nabla \cdot \boldsymbol{\sigma} - \frac{m^* n}{\tau}\mathbf{u} = 0, \tag{1b}$$

where $\mathbf{u}$ is the macroscopic velocity of fluid elements, $\boldsymbol{\sigma} = \eta[\nabla \otimes \mathbf{u} + (\nabla \otimes \mathbf{u})^T - (\nabla \cdot \mathbf{u})I]$ is the shear stress tensor. We have neglected pressure gradients because, assuming the "gradual channel approximation," they result in a negligible correction to the capacitance between the 2DEG and the gates, and can be absorbed into the electric potential. The bulk viscosity of electrons is considered negligible [22,51]. Equation (1) is supplemented by boundary conditions, which are determined by the magnitude and direction of current flowing in and out of the 2DEG at the inner and outer electrodes.

We also omitted the nonlinear convective derivative (Navier term) $\mathbf{u} \cdot \nabla\mathbf{u}$ on account of the very low Reynolds number (<0.1) in the electron fluid. At temperatures when hydrodynamic effects become prominent, thermal motion of electrons become sufficiently strong that effects of Landau quantization are negligible. Furthermore, the Hall viscosity compares to the shear viscosity by a factor of $2\omega_c\tau_{ee}$ [20]. From values in Table I, this is ≈0.16, which we assume is small and therefore, negligible.

For the case of homogeneous charge density and assuming azimuthal symmetry, with the convention $\mathbf{u} = u\hat{\mathbf{r}} + v\hat{\boldsymbol{\phi}}$, the exact solution of (1) is given by [38,52]

$$u(r) = u_1 r_1/r, \tag{2a}$$

$$v(r) = c_1 I_1(r/D) + c_2 K_1(r/D) - \omega_c \tau u_1 r_1/r, \tag{2b}$$

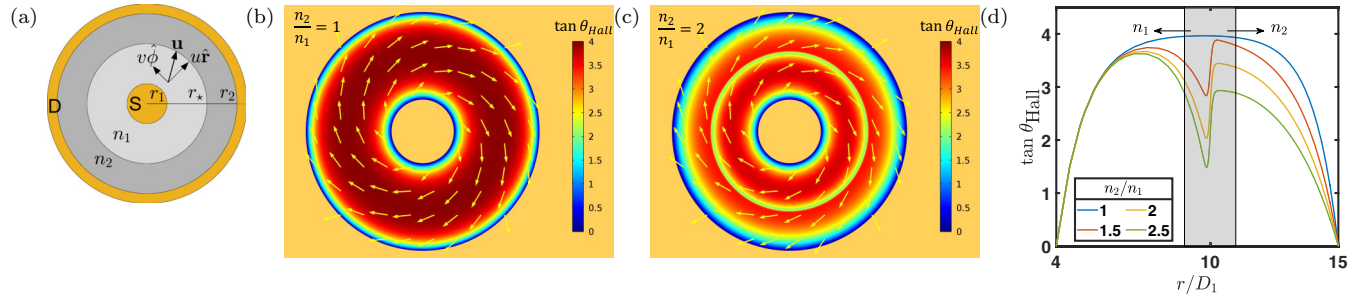

FIG. 1. (a) Schematic of the setup considered in this paper. [(b) and (c)] Colormap of $\tan\theta_{\rm Hall} = v(r)/u(r)$ for uniform density ($n_2/n_1 = 1$), and a density gradient $n_2/n_1 = 2$, obtained from a numerical simulation of the hydrodynamic equations (1) in COMSOL. The Hall angle is expected to be approximately constant in the bulk where flow is Drude-like, and change towards the contacts due to drag forces acting on the electrons due to viscous layers. A density gradient induces formation of additional viscous layers at the interface, sensitive to the density gradient. (d) Radial profile [along a radial section of (c)] of $\tan\theta_{\rm Hall}$ for various outer densities n_2. The interface induces a change in Hall angle in a region (shaded) approximately wide as the Gurzhi length D on either side. The jump in Hall angle at the interface also increases for a higher density gradient.

where $\omega_c = eB/m^*$ is the cyclotron frequency, $D = \sqrt{v\tau}$ is the Gurzhi length, I_1, K_1 are first-order modified Bessel functions, c_1, c_2 are constants determined by fitting to boundary conditions, and $u_1 = u(r_1)$ is the input radial velocity.

Comparing this with the nonviscous, simple Drude solution

$$v^{\rm ohm}(r) = -\omega_c \tau u_1 \frac{r_1}{r}, \tag{3}$$

we can see that viscosity conspires with momentum-relaxing scattering in the form of the Gurzhi length to affect the tangential velocity v. A simple way to highlight this effect is to calculate the local angle between the flow velocity and the radial vector, known as the Hall angle: $\tan\theta_{\rm Hall} = v(r)/u(r)$. For Drude flow [Eq. (3)], this is constant, while viscous terms in Eq. (2) cause deviations from it. At the source and drain, where flow is approximately normal to the surface of the leads, the Hall angle is zero, therefore, viscous layers develop near these terminals to accelerate the tangential flow.

In our case, we consider a nonuniform density profile $n(r)$ varying over a relatively small length scale $d \ll D$ at an interface at $r = r_\star$. In a gated junction in GaAs quantum wells, the density interface is expected to have a width $d \approx 100$ –150 nm. On solving the electrostatic potential due to the gates, we find the density varies as

$$n(r) = \frac{n_1 + n_2}{2} + \frac{n_2 - n_1}{2}\tanh([r - r_\star]/d), \tag{4}$$

which interpolates between the two regions $r < r_\star$ and $r > r_\star$ with densities n_1, n_2, respectively.

Given this density profile, we solve the hydrodynamic equations (1) in the numerical solver COMSOL, supplemented by no-slip conditions at the source and drain. We assume a density gradient in Eq. (4) that smoothly connects the two constant density regions over a characteristic length of $d = 0.1D \approx 100$ nm. Such a density setup can be created by using a dual gate architecture with top and bottom gates [53]. We assume Fermi-liquid behavior of electrons with respect to density, i.e., the e-e scattering rate goes as $\tau_{ee}^{-1} \propto 1/E_F \propto 1/n$. Also, given the high mobility of 2DEG, we assume the momentum-relaxing scattering is limited by phonons and not by disorder, therefore, τ is independent of n [22,54–56]. The Gurzhi length then varies as $D \propto n$. At hydrodynamic temperatures $l_{ee} \sim n$ [22] or even stronger, therefore qualitatively $D \sim n$ holds for a large range of parameters. We have assumed an electron-electron scattering length $l_{ee} = 300$ nm at $n_1 = 2 \times 10^{11}$ cm^{-2}, which corresponds to a temperature $T = 20$ K in 2DEG in GaAs/AlGaAs [22]. The Fermi temperature is $T_F = 83$ K, and the Fermi wave number and velocity, $k_F = (9\ \text{nm})^{-1}$, $v_F = 1.9 \times 10^7$ cm/s, assuming a parabolic dispersion of the conduction band. A summary of the values of parameters is given in Table I.

In Fig. 1, we plot the Hall angle profile for uniform density and a finite density gradient $n_2 = 2n_1$. We clearly see a change in the Hall angle near the density interface, indicating the formation of viscous layers. We also show the radial profile of $\tan\theta_{\rm Hall}$ for different density gradients. We find that a larger gradient causes a greater change in Hall angle, thereby creating stronger viscous layers.

The appearance of viscous boundary layers has already been shown in a graphene Corbino ring by mapping the Hall angle profile using single-electron transistor imaging [47]. Other techniques like nitrogen-vacancy center magnetometry have been used to map flow profiles of electrons in mesoscopic systems [57]. In light of such developments, we believe interface-induced viscous layers can also be observed by imaging the flow profile in experiments.

III. ANALYTIC DERIVATION OF TUNABLE VISCOUS LAYERS

The hydrodynamic equations (1) for homogeneous charge density are solved by Eq. (2). This form, although known in literature, is very nonintuitive. We show in Appendix A that it can be approximated by the much simpler expression

$$v(r) = (\omega_c\tau u_1 + v_1)\sqrt{\frac{r_1}{r}}e^{-(r-r_1)/D} - \omega_c\tau u_1\frac{r_1}{r} + (\omega_c\tau u_2 + v_2)\sqrt{\frac{r_2}{r}}e^{-(r_2-r)/D}, \quad r_2 > r_1 \gtrsim D, \tag{5}$$

where r_1, r_2 are the radii of the inner and outer contacts. This shows that there are two viscous layers exponentially localized over a length D at the inner and outer terminals at r_1, r_2, and a Drude contribution which dominates in the

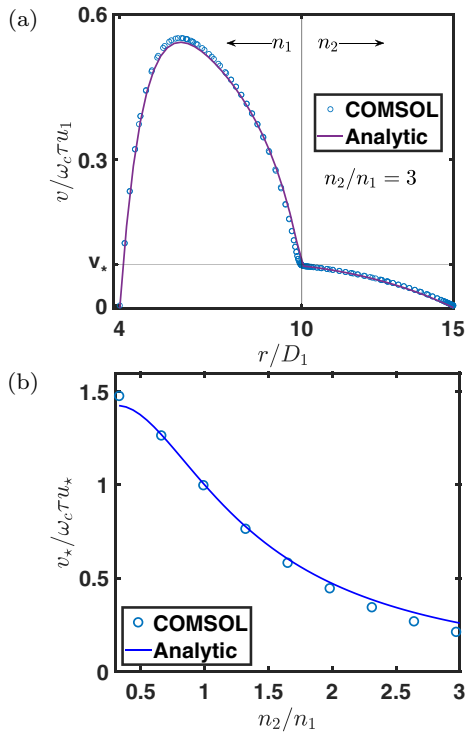

FIG. 2. (a) Plot of tangential flow velocity as function of radial distance from Eq. (6). Numerical simulation of Eq. (1) using COMSOL with smooth density gradient as in Eq. (4) with $d = 0.1D_1 \sim 100$ nm shows that the piecewise analytical solution with interface conditions approximates the flow very well. Viscous layers approximately wide as the Gurzhi length D act near the input, output terminals and at the interface to match the bulk Ohmic velocity to flow at the boundaries. Tuning the density ratio changes the tangential velocity at the interface, $v_\star$, which, in turn modulates the strength of viscous layers. (b) Velocity at interface as function of density ratio, obtained using analytic solution (6) and using boundary conditions (9), (10). $v_\star$ can be made to vary by a factor of 3 by varying n_2/n_1 over experimentally feasible ranges. COMSOL simulation of the Stokes flow with smooth interface gives identical values of $v_\star$ and verifies that our interface conditions are accurate.

bulk $r_1 + D \lesssim r \lesssim r_2 - D$. Surprisingly, if the injected velocity v_1 matches the nonviscous Drude value $v^{\text{ohm}}(r_1)$ in (3), Eq. (5) predicts that the viscous layers disappear completely. As noted earlier, metal-2DEG interfaces are almost always no-slip ($v_1, v_2 \approx 0$), so this situation is never realized.

For flow through a density gradient, the continuity equation constrains the radial velocity as $u(r) = n_1 r_1 u_1/n(r)r$. The bulk Ohmic velocity $v^{\text{ohm}} \sim -\omega_c\tau u(r)$ is therefore discontinuous at the interface, while the boundary condition (10) derived in the next section states that the net tangential velocity v must be continuous. Therefore viscous layers must develop at the interface at $r_\star$ to force v to a common value. Moreover, the viscous dissipation in these layers is proportional to the mismatch between the Drude velocity in the bulk and the interface velocity. By tuning the density ratio, we can tune this mismatch and thereby produce viscous layers of varying strengths.

In Fig. 2, we plot the velocity profile as a function of the radial distance r using the fit solution

$$v(r) = (\omega_c\tau u_1 + v_1)\sqrt{\frac{r_1}{r}}e^{-(r-r_1)/D_1} - \omega_c\tau u(r) + v^{\text{int}}(r) + (\omega_c\tau u_2 + v_2)\sqrt{\frac{r_2}{r}}e^{-(r_2-r)/D_2}, \quad (6)$$

where the velocity near the interface ($u_\star \equiv u(r_\star - d) = u_1 r_1/r_\star$)

$$v^{\text{int}}(r) = \begin{cases} (\omega_c\tau u_\star + v_\star)\sqrt{\frac{r_\star}{r}}e^{-(r_\star - r)/D_1} & r < r_\star \\ \left(\omega_c\tau u_\star \frac{n_1}{n_2} + v_\star\right)\sqrt{\frac{r_\star}{r}}e^{-(r-r_\star)/D_2} & r > r_\star \end{cases}.$$

We support this result with a numerical simulation of the Stokes flow in COMSOL. As it can be seen, our approximate solution bears excellent agreement with the exact result. Moreover, from boundary condition (9), we can equate the off-diagonal stress tensor $\sigma_{r\phi}$ at $r_\star$ to get the common velocity $v_\star$.

$$-\frac{v_\star}{\omega_c\tau u_\star} = \frac{1 + 2\rho_\star + 2\rho_\star\overline{n} - \overline{n}^2}{-3 + 2\rho_\star + 2\rho_\star\overline{n}^2 + 3\overline{n}^3}, \quad (7)$$

where $\rho_\star = r_\star/D_1$ and $\overline{n} = n_2/n_1$. A plot of $v_\star$ versus $\overline{n}$ is also shown. Numerical simulation of the flow across a smooth density gradient of width $d \ll D$ produces very similar results to the piecewise analytical solution matched with interface conditions.

Thus we see that by changing the density ratio, we can tune the velocity $v_\star$ at the interface, by which we can control the appearance of viscous layers. This also has implications in the electric resistance, as we explore in Sec. V.

IV. BOUNDARY CONDITIONS OF FLOW AT INTERFACE

We derive the boundary conditions on which our previous results are based. We consider a sharp interface between two regions of densities n_1 and n_2. By sharp, it is implied that the variation of density is over length d much smaller than the dimensions of the sample, but larger than the Fermi wavelength. To derive boundary conditions, we integrate the equations of flow (1a), (1b) over a patch with faces parallel to the interface. Because of the ϕ symmetry of the system, this is the same as integrating the equations from $r_\star - d$ to $r_\star + d$, where $2d$ is the thickness of the interface.

For the continuity equation,

$$\int_{r_\star - d}^{r_\star + d} dr\, \partial_r(rnu) = 0.$$

The radial velocity is therefore discontinuous, as

$$(nu)\Big|_{r_\star - d}^{r_\star + d} = 0. \quad (8)$$

Integrating the tangential component of (1b),

$$-eB\int_{r_\star - d}^{r_\star + d} rdr\, nu + \int_{r_\star - d}^{r_\star + d} dr\frac{\partial_r(r^2\sigma_{r\phi})}{r} - \frac{m^\star}{\tau}\int_{r_\star - d}^{r_\star + d} rdr\, nv = 0.$$

From the continuity equation, $r\,nu = \text{const}$, so, in the limit of small d, the first term gives a vanishing contribution. Similarly, assuming the tangential flow v does not diverge at the interface, the third term contributes negligibly in limit of small d. Therefore

$$0 \approx \frac{1}{r_\star}\int_{r_\star-d}^{r_\star+d} dr\ \partial_r(r^2\sigma_{r\phi}) = \frac{1}{r_\star}(r^2\sigma_{r\phi})\Big|_{r_\star-d}^{r_\star+d}.$$

In other words, the off-diagonal stress tensor, $\sigma_{r\phi}$, is continuous at the interface:

$$\sigma_{r\phi}\big|_{r_\star-d}^{r_\star+d} = 0. \tag{9}$$

Given $\sigma_{r\phi} = r\partial_r(v/r)$, this implies that the tangential flow velocity v is also continuous.

$$v\big|_{r_\star-d}^{r_\star+d} = 0. \tag{10}$$

Multiplying the radial component of (1b) by u and integrating,

$$-e\int_{r_\star-d}^{r_\star+d} rdr\ nu\partial_r\Phi + eB\int_{r_\star-d}^{r_\star+d} rdr\ nuv + \int_{r_\star-d}^{r_\star+d} dr\frac{u}{r}\partial_r(r^2\sigma_{rr}) - \frac{m^*}{\tau}\int_{r_\star-d}^{r_\star+d} rdr\ nu^2 = 0, \tag{11}$$

where Φ is the electric potential. Using the fact that $rnu = I/2\pi e = \text{const}$ across the interface, as before, we find that the terms proportional to B, τ^{-1} have a vanishing contribution in the limit of small d. The net condition reduces to

$$\Phi\Big|_{r_\star+d}^{r_\star-d} \times \frac{I}{2\pi} = (ru\sigma_{rr})\Big|_{r_\star+d}^{r_\star-d} + \int_{r_\star-d}^{r_\star+d} r\,dr\ \frac{\sigma_{rr}^2}{\eta}, \tag{12}$$

where integration by parts has been used for the right-hand side. Given $\sigma_{rr} = \eta r\partial_r(u/r)$, we find

$$(ru\sigma_{rr})\Big|_{r_\star+d}^{r_\star-d} = \left(\frac{I}{2\pi e}\right)^2\frac{2}{r_\star^2}\left(\frac{\eta_2}{n_2^2} - \frac{\eta_1}{n_1^2}\right). \tag{13}$$

Together with potential jump at the inner and outer contacts, this covers viscous dissipation in the homogeneous regions. The remaining term in Eq. (12) is just the viscous dissipation due to compressive flow at the interface. Neglecting derivative of r compared to n at the interface,

$$\int_{r_\star-d}^{r_\star+d} r\,dr\ \frac{\sigma_{rr}^2}{\eta} = \left(\frac{I}{2\pi e}\right)^2\int dr\ r^3\eta\left(\frac{d}{dr}\frac{1}{nr^2}\right)^2 \approx \left(\frac{I}{2\pi e}\right)^2\int\frac{\eta}{n^4 r}\left(\frac{dn}{dr}\right)^2 dr.$$

Finally, in the limit $d \to 0$, we can approximate

$$\left(\frac{dn}{dr}\right)^2 = \left(\frac{\Delta n}{2d}\right)^2\text{sech}^4\left(\frac{r-r_\star}{d}\right) \approx \frac{(\Delta n)^2}{3d}\,\delta(r-r_\star). \tag{14}$$

Using this in the integral for viscous dissipation, the total potential drop at the interface is

$$-\frac{\Delta\Phi^{\text{int}}}{I} = \frac{\eta_2}{\pi(n_2 e)^2 r_\star^2} - \frac{\eta_1}{\pi(n_1 e)^2 r_\star^2} + \frac{\eta_\star}{\pi(n_\star e)^2}\frac{1}{6r_\star d}\left(\frac{\Delta n}{n_\star}\right)^2, \tag{15}$$

where $\Delta n = n_2 - n_1$ is the difference in densities, $n_\star = (n_1 + n_2)/2$ is the density in the middle of the junction, and $\eta_\star = m^* n_\star \times v_F(n_\star) l_{ee}(n_\star)/4$ is the corresponding shear viscosity.

Equations (8), (9), (10), and (15) are the required boundary conditions of the problem.

V. SIGNATURE OF VISCOUS LAYERS IN MAGNETORESISTANCE

In Fig. 3, we plot the magnetoresistance $\Delta R = R(B) - R(0)$ versus n_2/n_1, calculated numerically for a high mobility $\mu = 2\times10^6 \text{cm}^2/(\text{V s})$ and a low mobility $\mu = 2000\ \text{cm}^2/(\text{V s})$ Corbino ring. Assuming a ultrahigh mobility sample where momentum-relaxing scattering is due to phonons only, the mobility should be close to our assumed high mobility value at $T \approx 20$ K [22]. It must be noted that in the Corbino, voltage applied divided by current yields the inverse of magnetoconductance, which is not equal to the magnetoresistance as the conductivity tensor in a magnetic field is nondiagonal. However, in the following, we use inverse magnetoconductance and magnetoresistance interchangeably for convenience.

For nonviscous flow, described by the Drude equation, the resistance for the density junction is simply

$$\Delta R^{\text{ohm}} = (\omega_c\tau)^2\frac{R_1^{\text{Dru}}}{2\pi}\left[\ln\left(\frac{r_\star}{r_1}\right) + \frac{n_1}{n_2}\ln\left(\frac{r_2}{r_\star}\right)\right], \tag{16}$$

where the Drude resistivity $R_1^{\text{Dru}} = m^*/n_1 e^2\tau = 15.3\ \Omega$ for values of parameters in Table I. When scaled by $(\omega_c\tau)^2 R_1^{\text{Dru}} (= 244\Omega)$, the magnetoresistance versus n_2/n_1 for samples with different mobility should collapse onto a single curve. This is clearly reflected in the result for the low mobility simulation in Fig. 3. However, we find that the presence of viscous layers serve to suppress this magnetoresistance. This is counter intuitive, given that viscous dissipation increases, but by decelerating the velocity at the interface, the viscous layers reduce the Ohmic dissipation as well.

To describe this analytically, we start with the power dissipation for hydrodynamic flow:

$$I\Delta\Phi^{\text{bulk}} + \oint \mathbf{u}\cdot\boldsymbol{\sigma}\cdot d\mathbf{S} = \frac{1}{\tau}\int m^* n\mathbf{u}^2 dV + \int\frac{\boldsymbol{\sigma}^2}{2\eta}dV. \tag{17}$$

The first term on the left is the rate of work done by the electric potential to drive the current, while the second term is the rate of work done against the boundary stress. The energy provided by these terms are dissipated by Ohmic and viscous forces, described by the terms on the right-hand side. The importance of boundary stress is apparent if we consider the particular case of pure radial flow with no Ohmic dissipation [33]. It can be shown that in this case, the potential drop

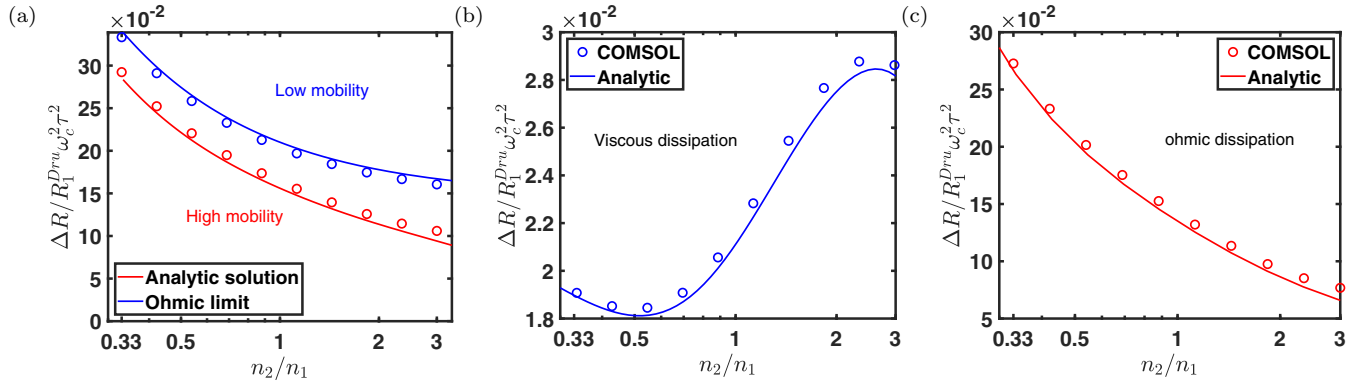

FIG. 3. (a) Scaled magnetoresistance $[R(B) - R(0)]/(R_1^{\mathrm{Dru}}\omega_c^2\tau^2)$ with density ratio. The circles are numerical simulation values from COMSOL, obtained by calculating the potential difference between inner and outer electrodes. The red solid line is an analytical plot of sum of viscous and Ohmic dissipation [see Eq. (17)]. For nonviscous flow, scaled magnetoresistance for different mobilities collapse onto a single curve [the Ohmic limit, Eq. (16)]. For high-mobility sample, viscous layers at the terminals and at interface suppress magnetoresistance (red curve). x axis is set to log scale to give equal emphasis to the cases $n_2 > n_1$ and $n_2 < n_1$. (b) Resistance due to viscous dissipation, calculated from COMSOL and from analytic solution (6) (expression in Table II). Because viscosity is proportional to density, viscous dissipation goes up with n_2/n_1. At very high n_2, velocity gradient in the bulk is low, resulting in a decrease in viscous resistance. The opposite happens for very low n_2. (c) Resistance due to Ohmic dissipation. In the bulk, the magnitude of current density, $|J| \sim J^{\mathrm{in}}(1 + \omega_c^2\tau^2)$ is approximately constant, so the Ohmic resistance per unit area $R^{\mathrm{ohm}} = J^2/\mu ne$ goes down monotonically with n_2.

$\Delta\Phi^{\mathrm{bulk}} = 0$, whereas power dissipation by viscous forces is finite. The only way the dissipated power can be compensated is by the boundary term on the left-hand side. Here, we expand this to a broader framework involving the effect of tangential velocity (caused by magnetic field) and effect of disorder.

When $B = 0$, the flow is radial and the viscous and Ohmic dissipation are decoupled in the electric resistance. By solving the Stokes equation, we find

$$R(0) = R^{\mathrm{vis}}(0) + R^{\mathrm{ohm}}(0),$$
$$R^{\mathrm{vis}}(0) = \frac{\eta_1}{\pi(n_1 e)^2}\frac{1}{r_1^2} - \frac{\eta_2}{\pi(n_2 e)^2}\frac{1}{r_2^2} + R^{\mathrm{vis,int}},$$
$$R^{\mathrm{ohm}}(0) = \frac{R_1^{\mathrm{Dru}}}{2\pi}\ln\frac{r_\star}{r_1} + \frac{R_2^{\mathrm{Dru}}}{2\pi}\ln\frac{r_2}{r_\star}. \quad (18)$$

The first term in $R^{\mathrm{vis}}(0)$ is due to the potential drop at the inner lead, the second term is from the outer lead and $R^{\mathrm{vis,int}}$ is due to the potential difference at the interface, determined by Eq. (15). This energy is dissipated by viscous forces in the regions of homogeneous charge density and due to compressive flow at the interface. For parameters in Table I and $n_2 = 3n_1$, we find the boundary resistance at the inner and outer leads is 0.24 Ω while the resistance arising due to potential jump at the interface is 1.76 Ω, i.e., the total viscous resistance is $R^{\mathrm{vis}}(0) = 2.0$ Ω. On the other hand, the zero-field Ohmic dissipation $R^{\mathrm{ohm}}(0)$ is 2.6 Ω. This conforms well with numerical values of viscous and Ohmic dissipation [in Eq. (17)] from our COMSOL simulation (2.3 and 2.6Ω, respectively).

A magnetic field couples the viscous and Ohmic dissipation in the electric potential and writing an analytical expression for resistance becomes difficult. However, based on our simplified solution (6), we can still derive approximate analytic expressions, as summarised in Table II. We find that the magnetic field contribution is proportional to $(\omega_c\tau)^2 = 16$ and is therefore larger than the zero-field resistance (7.15 Ω for viscous and 19.2 Ω for Ohmic dissipation, from COMSOL). From our simplified expressions, we can quantitatively break up the power dissipation into spatially localized channels. From inner to outer, they are: (i) boundary resistance at the inner lead due to viscous stresses acting on radial flow, (ii) resistance from viscous layer located $\sim D_1$ from the inner lead, arising due to tangential velocity, (iii) potential drop in bulk, primarily due to Ohmic scattering, (iv) resistance from viscous layers near the density interface, due to tangential velocity, (v) viscous dissipation due to radial compressive

TABLE II. Magnetoresistance due to bulk Ohmic flow and due to viscous layers, using approximate solution (6). If $\tilde{v}_i = -\frac{v(r_i)}{u(r_i)\omega_c\tau}$, $i = 1, 2$ for the inner and outer contacts, respectively, and $\tilde{v}_{\star\pm} = -\frac{v_\star}{u(r_\star \pm d)\omega_c\tau}$, then $\alpha_1 = (\tilde{v}_1 - 1)(1 + \frac{3D_1}{2r_1})$, $\alpha_2 = (\tilde{v}_2 - 1)(1 - \frac{3D_2}{2r_2})$, $\alpha_{\star\mp} = (\tilde{v}_{\star\mp} - 1)(1 \pm \frac{3D_1}{2r_\star})$, $\beta_i = \frac{1}{2}(\tilde{v}_i - 1) + 2(\tilde{v}_i - 1)^2$, $i = 1, 2, \star\pm$. $\tilde{v}_1, \tilde{v}_2 = 0$ in our simulations, $\tilde{v}_\star$ is given by Eq. (7). The expression for I_1 is given in Eq. (B1) in the Appendix.

$\Delta R(B)$	Viscous	Ohmic
bulk	$(\omega_c\tau)^2 \times R^{\mathrm{vis}}(0)$	$(\omega_c\tau)^2 \times R^{\mathrm{ohm}}(0)$
bdy layer	$\frac{\eta_1(\omega_c\tau)^2}{\pi(n_1 e)^2}\left[I_1 + \frac{\alpha_{\star-}^2}{4r_\star D_1} + \frac{2\alpha_{\star-}}{r_\star^2}\right]$ $+\frac{\eta_2(\omega_c\tau)^2}{\pi(n_2 e)^2}\left[\left(\frac{\alpha_{\star+}^2}{4r_\star} + \frac{\alpha_2^2}{4r_2}\right)\frac{1}{D_2} + \frac{2\alpha_{\star+}}{r_\star^2} + \frac{2\alpha_2}{r_2^2}\right]$	$\frac{(\omega_c\tau)^2}{2\pi} \times \left[R_1^{\mathrm{Dru}} D_1\left(\frac{\beta_1}{r_1} + \frac{\beta_{\star-}}{r_\star}\right)\right.$ $\left. + R_2^{\mathrm{Dru}} D_2\left(\frac{\beta_{\star+}}{r_\star} + \frac{\beta_2}{r_2}\right)\right]$

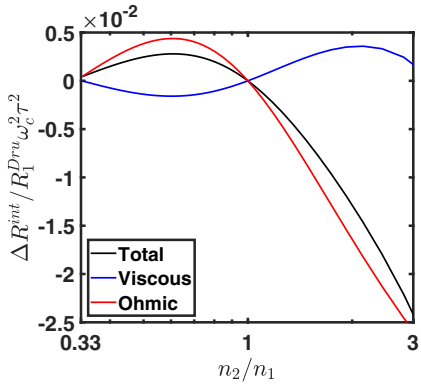

FIG. 4. Viscous, Ohmic and total contribution to magnetoresistance due to viscous layers at interface, obtained from analytic expressions in Table II. Negative values indicate that the viscous layers decrease magnetoresistance arising from momentum relaxing scattering. Because viscosity is proportional to density, viscous dissipation increases with n_2 near $n_2/n_1 = 1$. For high densities, velocity gradients in the viscous layers become small, therefore, viscous dissipation decreases. The opposite is true for very small n_2/n_1. Also because the viscous layers decelerate the flow more at the interface when n_2/n_1 is large, the Ohmic dissipation, which is proportional to $n|\mathbf{u}|^2$, decreases. For $n_2/n_1 < 1$, the opposite should be true, however, at very low n_2/n_1, the decrease in n becomes the overriding factor in Ohmic dissipation, and the Ohmic contribution starts to fall.

flow at the interface, (vi) bulk resistance due to Ohmic scattering in the outer region, followed by the outer viscous layer and the boundary resistance at the outer lead.

Our expressions in Table II allows us to separately calculate the contributions to the total resistance from the different viscous layers, something that would not be possible from either a global measurement or a numerical simulation which probes the total voltage drop and current across the entire device. In Fig. 4, we plot the dissipation from the expressions in Table II. We find that for $n_2 > n_1$, the net contribution from the interface viscous layers is negative, while for $n_2 < n_1$, it is positive. A heuristic explanation can be given as follows. Because viscosity is proportional to density, near $n_2/n_1 = 1$, viscous dissipation at interface layers increases with n_2. For very high densities, however, the velocity gradients in these layers is small, resulting in decrease in dissipation. The converse happens when $n_2 < n_1$. On the other hand, the Ohmic dissipation, which goes as $n|\mathbf{u}|^2$, drops with increasing density because the velocity of charge carriers decreases. For $n_2/n_1 < 1$, the increase in $|\mathbf{u}|$ due to decrease in n saturates, and the Ohmic dissipation starts to decrease due to decrease in n_2. The Ohmic contribution dominates over the viscous one, therefore, the net contribution to magnetoresistance from the viscous layers is negative when $n_2/n_1 > 1$ and positive when $n_2/n_1 < 1$.

VI. SUMMARY

We have studied hydrodynamic electron flow across density junctions in the Corbino geometry. Starting from the Stokes and continuity equations, we have derived boundary conditions of flow across the interface. Using these conditions, we have shown that we can make tunable viscous layers at the interface by varying the density ratio of the junction. We have also calculated the viscous and Ohmic dissipations by these viscous layers and we have found opposing behavior when electrons flow from regions of lower or higher density to the other.

We have based our analysis on experimentally tested values of viscosity and momentum relaxation mean free path at $T/T_F \sim 0.25$ in a 2DEG with parabolic dispersion, as well as a realistic system size. It is interesting to note that a novel "super-Fermi liquid" regime is predicted at $T/T_F \lesssim 0.16$ due to long-lived odd angular modes of the electron distribution function [58,59]. The theory predicts a linear-in-temperature dependence of conductivity, and an anomalous scaling of local conductivity with characteristic length scale of action of viscous forces [60]. The super-FL theory should be most distinct at low T when the deviation of the decay of long-lived modes of the distribution function from standard Fermi-liquid behavior is most apparent. At hydrodynamic temperatures considered here ($T/T_F \gtrsim 0.25$), such effects are expected to be mitigated. Hence we conclude that the standard hydrodynamic theory used in this paper suffices to explain our results.

Nevertheless, it would be an interesting idea to explore the effects of the new regime on viscous layers at lower temperatures. The effects of magnetic field and density modulation in the super FL regime is currently an open question and will be the subject of future research.

Density modulation in Corbino using top gates have been achieved in experiments [53]. Although Ref. [53] studies the ballistic regime, we can smoothly switch from it to the hydrodynamic regime using temperature as a tuning parameter. This presents the interesting problem of addressing the transport characteristics at this crossover. Study of thermal transport due to viscous layers is another possible avenue of investigation, especially for sample near charge neutrality [34,35]. Additionally, one could thread a magnetic flux through the Corbino like in the quantum Hall setup, as in Ref. [36]. Therefore our results presented in this paper open up possibilities for exploring novel transport phenomena in the Corbino geometry, and in general in the field of viscous electronic engineering.

ACKNOWLEDGMENTS

We are grateful to Giovanni Vignale for valuable discussions and for collaboration on a closely related project. We thank Alexander Hamilton for valuable discussions and experimental insights. This work was supported by the Singapore National Research Foundation Investigator Award (NRF-NRFI06-2020-0003) and the Australian Research Council Centre of Excellence in Future Low-Energy Electronics Technologies (CE170100039).

APPENDIX A: DERIVATION OF APPROXIMATE SOLUTION OF STOKES FLOW

The exact solution of Stokes equation (1b) is given by (2). Here, we derive the simplified form (5). Assuming $r_1, r_2 \gtrsim D$, we approximate the Bessel functions appearing in the solution

by their asymptotic forms. K_1 is a decreasing function, hence its contribution towards the outer boundary is small, i.e.,

$$v|_{r\to r_2} \approx c_1 I_1(r/D) + v^{\text{ohm}}(r) \approx c_1 \frac{e^{r/D}}{\sqrt{2\pi r/D}} + v^{\text{ohm}}(r).$$

Fitting this to the output flow at r_2,

$$v|_{r\to r_2} \approx (\omega_c\tau u_2 + v_2)\sqrt{\frac{r_2}{r}}e^{-(r_2-r)/D} - \omega_c\tau\frac{u_2 r_2}{r}.$$

We find that viscous correction to the Ohmic flow predominates in a region of width $\approx D$ from the outer boundary.

Similarly, because I_1 is an increasing function of r, and given that inner and outer boundaries are largely separated, we expect the relative contribution of I_1 towards inner boundary is small.

$$v|_{r\to r_1} \approx c_2 K_1(r/D) + v^{\text{ohm}}(r) \approx c_2\sqrt{\frac{\pi D}{2r}}e^{-r/D} + v^{\text{ohm}}(r).$$

Fitting to input flow at r_1:

$$v|_{r\to r_1} \approx (\omega_c\tau u_1 + v_1)\sqrt{\frac{r_1}{r}}e^{-(r-r_1)/D} - \omega_c\tau\frac{u_1 r_1}{r}.$$

Stitching these together in (2), we get the required expression.

Although the above approximations hold for $D \lesssim r_1$, a similar approach can be made for $r_1 \lesssim D$ (r_2 large). This situation, seemingly impractical, is now a possibility with the fabrication of ultraclean semiconductor heterojunctions. In recent experiments, mobilities as high as 50×10^6 cm^2/(V s) have been reached [61], for which the Gurzhi length is of the order of 10 μm. To simplify the Stokes solution, we assume a hypothetical interface at $r_\star = r_1 + D$ and divide the solution into two regions. The outer region, similar to before, has the form

$$v^{\text{out}} \approx (\omega_c\tau u_\star + v_\star)\sqrt{\frac{r_\star}{r}}e^{-(r-r_\star)/D} - \omega_c\tau\frac{u_1 r_1}{r} + (\omega_c\tau u_2 + v_2)\sqrt{\frac{r_2}{r}}e^{-(r_2-r)/D}. \tag{A1}$$

For the inner region $r_1 < r < r_\star$, we make small-argument expansion of the Bessel functions in the exact solution (2):

$$v^{\text{in}} = A\frac{r}{r_1} + A'\frac{r_1}{r} + A'\frac{r_1}{2}r\ln\frac{r}{r_1} + O(r^2/D^2),$$

where coefficients A, A' have been suitably defined to impose boundary conditions. Matching the flow at the input terminal,

$$v^{\text{in}} = (v_1 - A)\frac{r_1}{r} + A\frac{r}{r_1} + \frac{r_1}{2D^2}(v_1 - A + \omega_c\tau u_1)r\ln\frac{r}{r_1}. \tag{A2}$$

The remaining unknown A can be determined numerically by imposing continuity of vorticity at $r_\star$. The complete solution (A1), (A2) is plotted in Fig. 5 for the hypothetical case of different injected tangential velocities. The approximate analytic solution is also compared with the exact solution (2).

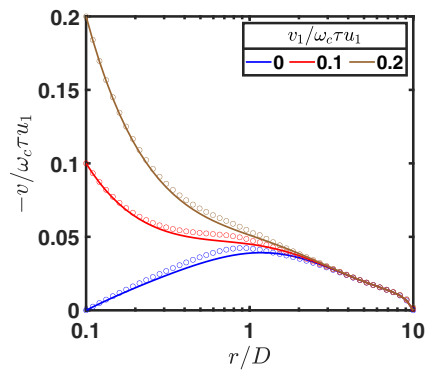

FIG. 5. Approximate solution of Stokes flow (circles) for different injected velocities when $r_1 \lesssim D$. Solid lines represent the exact solution

APPENDIX B: DERIVATION OF MAGNETORESISTANCE EXPRESSIONS IN TABLE II

1. Ohmic dissipation

From the power budget equation (17), the Ohmic power dissipation is

$$P^{\text{ohm}} = 2\pi m^*\tau^{-1}\int rn(u^2+v^2)dr.$$

First, let us consider homogeneous charge density. The radial component is simply $u = u_1 r_1/r$, hence, the corresponding contribution to P^{ohm} is

$$P^{\text{ohm},r} = I^2\frac{R^{\text{Dru}}}{2\pi}\ln\frac{r_2}{r_1},$$

where the total current $I = 2\pi r_1 neu_1$ and $R^{\text{Dru}} = m^*/ne^2\tau$.

From approximate solution (5), we can split the tangential velocity into a bulk Ohmic contribution and a boundary contribution as

$$v = v^{\text{ohm}} + v^{\text{bdy}},$$

where $v^{\text{bdy}} \propto e^{-(r-r_1)/D}$ near r_1 and $v^{\text{bdy}} \propto e^{-(r_2-r)/D}$ near r_2. From this, the tangential flow contribution to P^{ohm} is

$$P^{\text{ohm},t} = \frac{2\pi m^* n}{\tau}\left\{\int r(v^{\text{ohm}})^2 dr + \int r[2v^{\text{ohm}}v^{\text{bdy}} + (v^{\text{bdy}})^2]dr\right\}.$$

The first term, which is an Ohmic contribution and comes from the bulk, is

$$P^{\text{ohm},t}\Big|_{\text{bulk}} = I^2(\omega_c\tau)^2\frac{R^{\text{Dru}}}{2\pi}\ln\frac{r_2}{r_1} = (\omega_c\tau)^2 P^{\text{ohm},r} = (\omega_c\tau)^2 P^{\text{ohm}}\Big|_{B=0}.$$

The remaining contribution, coming from the viscous boundary layers, is

$$\begin{aligned} P^{\mathrm{ohm},t}\Big|_{\text{inner bdy}} &\times \frac{\tau}{2\pi m^* n} \\ &= -2\omega_c\tau u_1 r_1 (v_1 + \omega_c\tau u_1)\int_{r_1}^{\infty} e^{-(r-r_1)/D} dr \\ &\quad + r_1 (v_1 + \omega_c\tau u_1)^2 \int_{r_1}^{\infty} e^{-2(r-r_1)/D} dr \\ &= (\omega_c\tau u_1)^2 r_1 D\left\{2(\tilde{v}_1 - 1) + \frac{1}{2}(\tilde{v}_1 - 1)^2\right\} \end{aligned}$$

with the notation $\tilde{v}_1 = -v_1/\omega_c\tau u_1$. An exactly similar calculation gives

$$\begin{aligned} P^{\mathrm{ohm},t}\Big|_{\text{outer bdy}} &\times \frac{\tau}{2\pi m^* n} \\ &= (\omega_c\tau u_2)^2 r_2 D\left\{2(\tilde{v}_2 - 1) + \frac{1}{2}(\tilde{v}_2 - 1)^2\right\} \end{aligned}$$

with $u_2 = u(r_2) = u_1 r_1/r_2$, and $\tilde{v}_2 = -v_2/\omega_c\tau u_2$.

The generalization to a system with two different densities is straightforward: the power dissipated is the sum of the dissipations from each of the uniform density regions. The result is given in Table II.

2. Viscous dissipation

$$P^{\mathrm{vis}} = 2\pi \int \frac{\boldsymbol{\sigma}^2}{2\eta} r\, dr.$$

Under azimuthal symmetry, $\sigma_{rr} = -\sigma_{\phi\phi} = \eta r \partial_r (u/r)$, while $\sigma_{r\phi} = \sigma_{\phi r} = \eta r \partial_r (v/r)$. The viscous dissipation due to radial flow

$$P^{\mathrm{vis},r} = \frac{2\pi}{\eta}\int \sigma_{rr}^2 r\, dr = I^2 \frac{\eta}{\pi (ne)^2}\left(\frac{1}{r_1^2} - \frac{1}{r_2^2}\right).$$

This is the same as power supplied due to boundary stresses in the clean limit, when the electric field driving the current disappears [33]. The magnetic field correction, and also the contribution from disorder, comes from the azimuthal flow, as

$$\begin{aligned} P^{\mathrm{vis},t} &= \frac{2\pi}{\eta}\int \sigma_{r\phi}^2 r\, dr \\ &= 2\pi\eta\left\{\int_{r_1}^{r_2} r^3\left[\partial_r\left(\frac{v^{\mathrm{ohm}}}{r}\right)\right]^2 dr \right. \\ &\quad + \int_{r_1}^{r_2} r^3\left[2\partial_r\left(\frac{v^{\mathrm{ohm}}}{r}\right)\partial_r\left(\frac{v^{\mathrm{bdy}}}{r}\right)\right. \\ &\quad \left.\left. + \partial_r\left(\frac{v^{\mathrm{bdy}}}{r}\right)^2\right] dr\right\}. \end{aligned}$$

Like for Ohmic dissipation, the first term is proportional to the zero B field (bulk) resistance

$$P^{\mathrm{vis},t}|_{\mathrm{bulk}} = (\omega_c\tau)^2 P^{\mathrm{vis},r}.$$

The contribution from the boundary layers comes from the second term. At the inner boundary layer,

$$\begin{aligned} P^{\mathrm{vis},t}\Big|_{\text{inner bdy}} &= I^2 \frac{\eta(\omega_c\tau)^2}{\pi(ne)^2}\left\{\int_{r_1}^{\infty} F_1(r) e^{-(r-r_1)/D} dr \right. \\ &\quad \left. + \int_{r_1}^{\infty} F_2(r) e^{-2(r-r_1)/D} dr\right\}, \\ F_1(r) &= \frac{4}{r_1^{1/2} r^{3/2}}(\tilde{v}_1 - 1)\left(1 + \frac{3D}{2r}\right), \\ F_2(r) &= \frac{1}{r_1}(\tilde{v}_1 - 1)^2\left(1 + \frac{3D}{2r}\right)^2 \end{aligned}$$

with $\tilde{v}_1 = -v_1/\omega_c\tau u_1$ as before. If $r_1 \gg D$, F_1, F_2 are slowly varying with r compared to the exponential, hence, we may set their values as fixed at r_1.

$$\begin{aligned} P^{\mathrm{vis},t}\Big|_{\text{inner bdy}} &= I^2 \frac{\eta}{\pi(ne)^2}\left\{\frac{2\alpha_1}{r_1^2} + \frac{\alpha_1^2}{4r_1 D}\right\} \\ \alpha_1 &= (\tilde{v}_1 - 1)\left(1 + \frac{3D}{2r_1}\right). \end{aligned}$$

A very similar expression holds at r_2:

$$\begin{aligned} P^{\mathrm{vis},t}\Big|_{\text{outer bdy}} &= I^2 \frac{\eta(\omega_c\tau)^2}{\pi(ne)^2}\left\{\frac{2\alpha_2}{r_2^2} + \frac{\alpha_2^2}{4r_2 D}\right\} \\ \alpha_2 &= (\tilde{v}_2 - 1)\left(-1 + \frac{3D}{2r_1}\right). \end{aligned}$$

The dissipation due to two density regions is the sum of dissipation from each region; however, for our choice of parameters $r_1 = 4D$, the assumption $r_1/D \gg 1$ is not valid and naively using the above expression gives inaccurate estimates near r_1. In this case, we directly integrate the full expression keeping the generic form of $F_1(r), F_2(r)$. The result can be expressed in terms of the exponential integral function:

$$\begin{aligned} P^{\mathrm{vis},t}\Big|_{\text{inner bdy}} &= I^2 \frac{\eta(\omega_c\tau)^2}{\pi(ne)^2} I_1, \\ I_1 &= \left\{\frac{2(\tilde{v}_1 - 1)}{r_1^2} + \frac{(\tilde{v}_1 - 1)^2}{4r_1 D}\left(1 + \frac{3D}{2r_1}\right) + \lambda\right\}, \\ \lambda &= \frac{3}{4r_1^2}(\tilde{v}_1 - 1)^2\left(1 + \frac{r_1}{D} e^{2r_1/D}\mathrm{Ei}\left[-\frac{2r_1}{D}\right]\right), \\ \mathrm{Ei}[z] &= -\int_{-z}^{\infty} dt\; e^{-t}/t. \end{aligned} \tag{B1}$$

[1] R. N. Gurzhi, Sov. Phys. Usp. **11**, 255 (1968).
[2] R. N. Gurzhi, Zh. Eksp. Teor. Fiz. **44**, 771 (1963) [JETP **17**, 521 (1963)].
[3] R. N. Gurzhi, A. N. Kalinenko, and A. I. Kopeliovich, Phys. Rev. Lett. **74**, 3872 (1995).
[4] D. Y. H. Ho, I. Yudhistira, N. Chakraborty, and S. Adam, Phys. Rev. B **97**, 121404(R) (2018).
[5] D. Bandurin, I. Torre, R. K. Kumar, M. B. Shalom, A. Tomadin, A. Principi, G. Auton, E. Khestanova, K. Novoselov, I. Grigorieva, L. Ponomarenko, A. Geim, and M. Polini, Science **351**, 1055 (2016).
[6] A. D. Levin, G. M. Gusev, E. V. Levinson, Z. D. Kvon, and A. K. Bakarov, Phys. Rev. B **97**, 245308 (2018).
[7] C. Tan, D. Y. H. Ho, L. Wang, J. I. A. Li, I. Yudhistira, D. A. Rhodes, T. Taniguchi, K. Watanabe, K. Shepard, P. L. McEuen, C. R. Dean, S. Adam, and J. Hone, Sci. Adv. **8**, eabi8481 (2022).
[8] L. Levitov and G. Falkovich, Nat. Phys. **12**, 672 (2016).
[9] A. Aharon-Steinberg, T. Völkl, A. Kaplan, A. K. Pariari, I. Roy, T. Holder, Y. Wolf, A. Y. Meltzer, Y. Myasoedov, M. E. Huber, B. Yan, G. Falkovich, L. S. Levitov, M. Hücker, and E. Zeldov, Nature (London) **607**, 74 (2022).
[10] J. A. Sulpizio, L. Ella, A. Rozen, J. Birkbeck, D. J. Perello, D. Dutta, M. Ben-Shalom, T. Taniguchi, K. Watanabe, T. Holder, R. Queiroz, A. Principi, A. Stern, T. Scaffidi, A. K. Geim, and S. Ilani, Nature (London) **576**, 75 (2019).
[11] M. J. H. Ku, T. X. Zhou, Q. Li, Y. J. Shin, J. K. Shi, C. Burch, L. E. Anderson, A. T. Pierce, Y. Xie, A. Hamo, U. Vool, H. Zhang, F. Casola, T. Taniguchi, K. Watanabe, M. M. Fogler, P. Kim, A. Yacoby, and R. L. Walsworth, Nature (London) **583**, 537 (2020).
[12] H. Guo, E. Ilseven, G. Falkovich, and L. S. Levitov, Proc. Natl. Acad. Sci. **114**, 3068 (2017).
[13] R. Krishna Kumar, D. A. Bandurin, F. M. D. Pellegrino, Y. Cao, A. Principi, H. Guo, G. Auton, M. Ben Shalom, L. A. Ponomarenko, G. Falkovich, K. Watanabe, T. Taniguchi, I. Grigorieva, L. S. Levitov, M. Polini, and A. Geim, Nat. Phys. **13**, 1182 (2017).
[14] L. V. Ginzburg, Y. Wu, M. P. Röösli, P. R. Gomez, R. Garreis, C. Tong, V. Stará, C. Gold, K. Nazaryan, S. Kryhin, H. Overweg, C. Reichl, M. Berl, T. Taniguchi, K. Watanabe, W. Wegscheider, T. Ihn, and K. Ensslin, Phys. Rev. Res. **5**, 043088 (2023).
[15] J. Crossno, J. K. Shi, K. Wang, X. Liu, A. Harzheim, A. Lucas, S. Sachdev, P. Kim, T. Taniguchi, K. Watanabe, T. A. Ohki, and K. C. Fong, Science **351**, 1058 (2016).
[16] J. Gooth, F. Menges, N. Kumar, V. Süß, C. Shekhar, Y. Sun, U. Drechsler, R. Zierold, C. Felser, and B. Gotsmann, Nat. Commun. **9**, 4093 (2018).
[17] A. Lucas and S. Das Sarma, Phys. Rev. B **97**, 245128 (2018).
[18] A. Jaoui, B. Fauqué, and K. Behnia, Nat. Commun. **12**, 195 (2021).
[19] S. Ahn and S. Das Sarma, Phys. Rev. B **106**, L081303 (2022).
[20] P. S. Alekseev, Phys. Rev. Lett. **117**, 166601 (2016).
[21] Q. Shi, P. D. Martin, Q. A. Ebner, M. A. Zudov, L. N. Pfeiffer, and K. W. West, Phys. Rev. B **89**, 201301(R) (2014).
[22] A. C. Keser, D. Q. Wang, O. Klochan, D. Y. H. Ho, O. A. Tkachenko, V. A. Tkachenko, D. Culcer, S. Adam, I. Farrer, D. A. Ritchie, O. P. Sushkov, and A. R. Hamilton, Phys. Rev. X **11**, 031030 (2021).
[23] A. T. Hatke, M. A. Zudov, J. L. Reno, L. N. Pfeiffer, and K. W. West, Phys. Rev. B **85**, 081304(R) (2012).
[24] R. G. Mani, A. Kriisa, and W. Wegscheider, Sci. Rep. **3**, 2747 (2013).
[25] G. M. Gusev, A. S. Jaroshevich, A. D. Levin, Z. D. Kvon, and A. K. Bakarov, Phys. Rev. B **103**, 075303 (2021).
[26] G. M. Gusev, A. D. Levin, E. V. Levinson, and A. K. Bakarov, Phys. Rev. B **98**, 161303(R) (2018).
[27] A. I. Berdyugin, S. G. Xu, F. M. D. Pellegrino, R. K. Kumar, A. Principi, I. Torre, M. B. Shalom, T. Taniguchi, K. Watanabe, I. V. Grigorieva, M. Polini, A. K. Geim, and D. A. Bandurin, Science **364**, 162 (2019).
[28] X. Wang, P. Jia, R.-R. Du, L. N. Pfeiffer, K. W. Baldwin, and K. W. West, Phys. Rev. B **106**, L241302 (2022).
[29] Y. Dai, R. R. Du, L. N. Pfeiffer, and K. W. West, Phys. Rev. Lett. **105**, 246802 (2010).
[30] A. T. Hatke, M. A. Zudov, L. N. Pfeiffer, and K. W. West, Phys. Rev. B **83**, 121301(R) (2011).
[31] M. Białek, J. Łusakowski, M. Czapkiewicz, J. Wróbel, and V. Umansky, Phys. Rev. B **91**, 045437 (2015).
[32] P. S. Alekseev and A. P. Alekseeva, Phys. Rev. Lett. **123**, 236801 (2019).
[33] M. Shavit, A. Shytov, and G. Falkovich, Phys. Rev. Lett. **123**, 026801 (2019).
[34] V. Gall, B. N. Narozhny, and I. V. Gornyi, Phys. Rev. B **107**, 235401 (2023).
[35] A. Levchenko, S. Li, and A. V. Andreev, Phys. Rev. B **106**, L201306 (2022).
[36] A. Tomadin, G. Vignale, and M. Polini, Phys. Rev. Lett. **113**, 235901 (2014).
[37] S. Li, A. Levchenko, and A. V. Andreev, Phys. Rev. B **105**, 125302 (2022).
[38] V. Gall, B. N. Narozhny, and I. V. Gornyi, Phys. Rev. B **107**, 045413 (2023).
[39] A. Rycerz, K. Rycerz, and P. Witkowski, Materials **16**, 4250 (2023).
[40] T. Scaffidi, N. Nandi, B. Schmidt, A. P. Mackenzie, and J. E. Moore, Phys. Rev. Lett. **118**, 226601 (2017).
[41] T. Holder, R. Queiroz, T. Scaffidi, N. Silberstein, A. Rozen, J. A. Sulpizio, L. Ella, S. Ilani, and A. Stern, Phys. Rev. B **100**, 245305 (2019).
[42] V. Panchal, A. Lartsev, A. Manzin, R. Yakimova, A. Tzalenchuk, and O. Kazakova, Sci. Rep. **4**, 5881 (2014).
[43] E. I. Kiselev and J. Schmalian, Phys. Rev. B **99**, 035430 (2019).
[44] J. N. Engdahl, A. C. Keser, and O. P. Sushkov, Phys. Rev. Res. **4**, 043175 (2022).
[45] A. C. Keser and O. Sushkov, Turk. J. Phys. **47**, 28 (2023).
[46] J. N. Engdahl, A. C. Keser, T. Schmidt, and O. P. Sushkov, Phys. Rev. B **109**, 195402 (2024).
[47] C. Kumar, J. Birkbeck, J. A. Sulpizio, D. Perello, T. Taniguchi, K. Watanabe, O. Reuven, T. Scaffidi, A. Stern, A. K. Geim, and S. Ilani, Nature (London) **609**, 276 (2022).
[48] A. D. Levin, G. M. Gusev, A. S. Yaroshevich, Z. D. Kvon, and A. K. Bakarov, Phys. Rev. B **108**, 115310 (2023).
[49] R. Moessner, N. Morales-Durán, P. Surówka, and P. Witkowski, Phys. Rev. B **100**, 155115 (2019).
[50] A. Hui, V. Oganesyan, and E.-A. Kim, Phys. Rev. B **103**, 235152 (2021).

[51] A. Principi, G. Vignale, M. Carrega, and M. Polini, Phys. Rev. B **93**, 125410 (2016).
[52] A. Levchenko and J. Schmalian, Ann. Phys. **419**, 168218 (2020).
[53] M. M. Elahi, H. Vakili, Y. Zeng, C. R. Dean, and A. W. Ghosh, Phys. Rev. Lett. **132**, 146302 (2024).
[54] V. K. Arora and A. Naeem, Phys. Rev. B **31**, 3887 (1985).
[55] B. K. Ridley, J. Phys. C **15**, 5899 (1982).
[56] T. Kawamura and S. Das Sarma, Phys. Rev. B **42**, 3725 (1990).
[57] A. Jenkins, S. Baumann, H. Zhou, S. A. Meynell, Y. Daipeng, K. Watanabe, T. Taniguchi, A. Lucas, A. F. Young, and A. C. Bleszynski Jayich, Phys. Rev. Lett. **129**, 087701 (2022).
[58] S. Kryhin and L. Levitov, Phys. Rev. B **107**, L201404 (2023).
[59] P. J. Ledwith, H. Guo, and L. Levitov, Ann. Phys. **411**, 167913 (2019).
[60] S. Kryhin, Q. Hong, and L. Levitov, arXiv:2310.08556 [cond-mat.mes-hall].
[61] Y. J. Chung, A. Gupta, K. W. Baldwin, K. W. West, M. Shayegan, and L. N. Pfeiffer, Phys. Rev. B **106**, 075134 (2022).